Proceedings of the 5th WSEAS Int. Conf. on Power Systems and Electromagnetic Compatibility, Corfu, Greece, August 23-25, 2005 (pp101-105)

DISCHARGE GEOMETRY BEHAVIOR IN NEGATIVE CORONA AT ATMOSPHERIC PRESSURE ON A CYLINDRICAL ARRANGEMENT

LILIANA ARÉVALO[1*], MARLEY BECERRA[2] FRANCISCO ROMÁN[1]
Electromagnetic Compatibility Research Group EMC – UN
[1]National University of Colombia, Bogotá, Colombia;
[2] Uppsala University, Uppsala, Sweden.
Ciudad Universitaria Unidad Camilo Torres Bloque 4 Of. 702 Bogotá – Colombia
COLOMBIA - SWEDEN
http://www.emc-un.unal.edu.co

Abstract:
A numerical study of a negative corona discharge in air at atmospheric pressure in a non – uniform electric field: A cylindrical arrangement with earthed inner electrodes is presented. Results were obtained by solving numerically Poisson's equation coupled with the continuity equations for electrons, positive, and negative ions, and considering the space – time evolution, as well as the electric field distribution and the current behaviour. The effects of ionization, attachment, recombination, electron diffusion are included. Calculations were made using a cylindrical discharge channel and a truncated cone. The calculated values were compared with the experimental results.

Key-Words:
Negative corona, Trichel pulse, continuity equations, Poisson equation, particles density, numerical techniques, field emission, ion bombardment, attachment, and recombination.

1. The theoretical "equations and parameters"

Many experimental results have shown that the discharge presents a filamentary geometry. However, some researchers have shown that the discharge geometry in low pressures is not quite filamentary. In order to determine and compare these possible discharge geometries, truncated cone geometry and cylindrical geometries were simulated. The theory is based on a classical "one – dimensional model" in which the continuity equations for electrons, positive ions, and negative ions are used to describe the axial discharge development:

$$\frac{\partial N_e}{\partial t} = N_e\alpha|W_e| - N_e\eta|W_e| - N_eN_p\beta - \frac{\partial(N_eW_e)}{\partial x} \qquad (1)$$

$$\frac{\partial N_P}{\partial t} = N_e\alpha|W_e| - N_eN_p\beta - N_nN_p\beta - \frac{\partial(N_pW_p)}{\partial x} \qquad (2)$$

$$\frac{\partial N_n}{\partial t} = N_e\eta|W_e| - N_nN_p\beta - \frac{\partial(N_nW_n)}{\partial x} \qquad (3)$$

Where t is time, x the distance from the cathode; Ne, Np and Nn are respectively the electron, positive ion, negative ion, and We, Wp and Wn correspond to electron, positive ion and negative ion drift velocities. The material functions α, β and η are the ionization, recombination and attachment respectively. Diffusion is not included, since its inclusion had negligible effect, as it was reported on the results of [5] and [7]. The continuity equations are coupled with Poisson's equation via the charge density.

$$\nabla^2\phi = -\frac{e}{\varepsilon}\left(N_p - N_e - N_n\right) \qquad (4)$$

Where: ε is the dielectric constant, e the electron charge and ϕ the electric potential. The electric field, E, is computed using $E = -\nabla\phi$ (5)

The axial electric field $E(x)$ is evaluated using the method of disks [7], which represent the discharge as a cylinder with a uniform radial distribution and variable axial charge distribution.

To start the computation at t_0, an electron density in Gaussian distribution was considered (10^3 cm^{-3}). A uniform mesh was used; the total number of axial mesh used to represent the 4 cm gap between the cathode and anode was 1500. Due to the computing time required, the mesh could not be finer. For the electric field calculation, a 4μm radial channel was simulated. .

In this paper Sato's equation [10] was used to calculate

the current I on the external circuit, due to the electrons and ions motion between the electrodes:

$$I = \frac{Ae}{V_a}\int_0^d \left(N_p W_p - N_n W_n - N_e W_e + D\frac{\partial N_e}{\partial x} \right) E_L \cdot dx \quad (9)$$

Here: V_a is the applied voltage, A is the cross sectional area of the discharge channel and E_L is the LaPlacian electric field.

2. Experiments and Results [13, 14]

The Trichel pulses development results are presented for the air atmospheric conditions in Bogotá, Colombia. The experimental setup consisted of a coaxial cylindrical arrangement with a corona-electrode, placed on the inner cylinder electrode surface and perpendicular to the inner cylinder electrode axis. The corona-electrode was a brass rod terminated on a hyperbolical tip with 0.15mm radius of curvature. The detailed measured current is shown in Fig. 1.

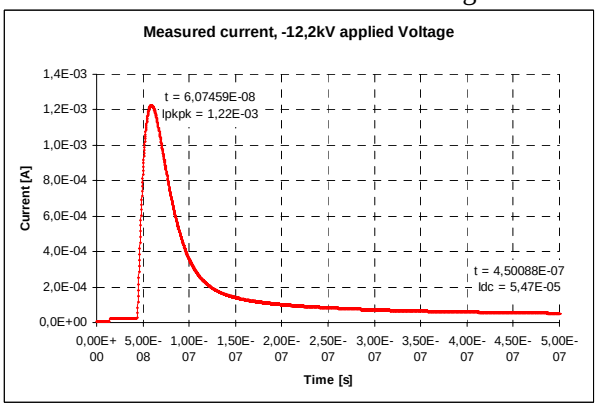

Fig. 1. Measured streamer at -12.2kV applied voltage. This signal was measured with a LeCroy oscilloscope model LC574AM.

2.1. Simulation Results

Fig. 2 shows, that the rise time is the same for both geometrical discharges, but the magnitudes of the peak and direct current components are different. For the conical discharge geometry the peak current value is 1.57mA and for the cylindrical discharge geometry is 1.22mA, the direct current component is 550μA in conical discharge channel and 37μA in the cylindrical geometry. It is important to notice that in the slow Trichel propagation stage (15 to 40ns); the external current of the conical geometry does not fall as the current of the cylindrical geometry does.

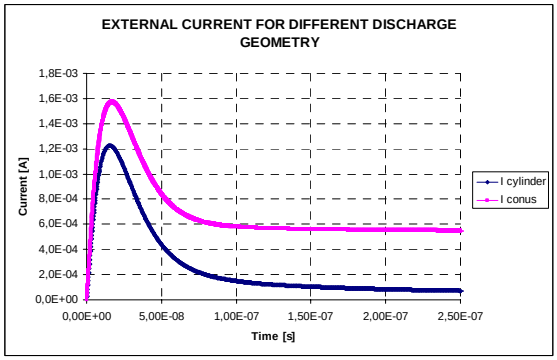

Fig. 2. Current behavior for different discharge geometry. Notice that peak and direct current values are different for each case.

For explain the existent differences in the external current circuit it is necessary to analyze the particles behavior in the different Trichel propagation stages: Space charge growth (13ns), slow Trichel propagation (40ns), Trichel pulse termination (79 and 150ns) and the Trichel pulse decay phase (254ns).

In the initial stage “Space charge growth” (Fig. 3) the particles density distributions are equal, they have identical magnitude and they are located in the same interelectrodic gap space. The unique difference is presented in the electric field magnitude and it is due to the different discharge radius. The electric field is inversely proportional to almost the square of the discharge radius, therefore in the conical geometry the discharge radius is minor than in the cylindrical geometry and that is why the electric field is higher in the conical geometry. Due to this electric field differences, the peak current is higher in the conical geometry than in the cylindrical.

In the slow Trichel propagation stage (40ns, Fig. 4.), the particles densities have the same magnitudes and location in the interelectrodic gap space. However, the electric field magnitude in the conical geometry is twice the electric field magnitude of the cylindrical discharge geometry. Due to this difference, the external current magnitude is higher in the conical geometry than in the cylindrical region.

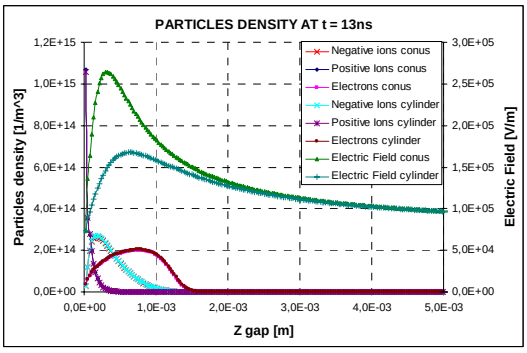

Fig. 3. Particles density at 13ns. Notice that waveforms are equals in both cases but the electric field magnitude is not.

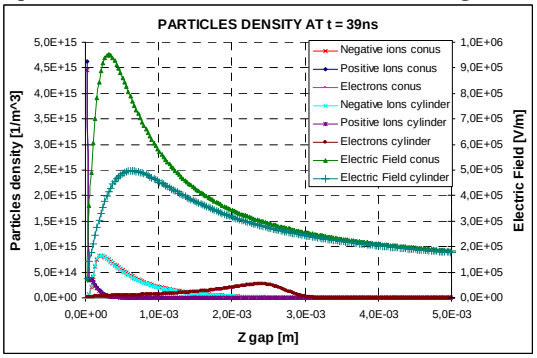

Fig. 4. Particles density at 39ns. Notice that conical discharge channel has a higher electric field than cylindrical channel.

For the Trichel pulse termination (79 and 150ns) stage, the external current behavior is different. The current in the conical discharge is at the beginning (~50ns) 3 times of the external current of the cylindrical geometry, and at the end (~150ns) of this stage is 5 times the current of the cylindrical geometry. Fig. 2 shows that for conical geometry the current starts to be constant in ~130ns. Fig. 5 shows that in 79ns the particles densities are still located in the same interelectrodic gap space and their magnitudes are equal, the unique difference between both calculations are the electric field that is higher for the conical geometry than the cylindrical discharge channel

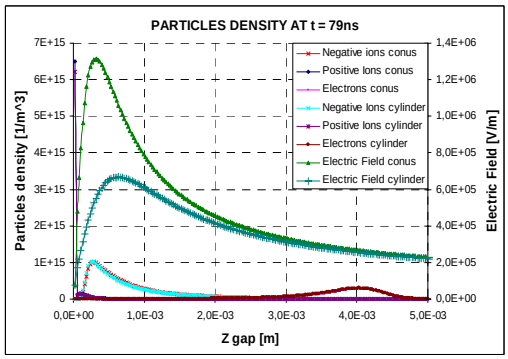

Fig. 5. Particles density at 79ns. Notice that particles density in both geometries are located in the same interelectrodic region.

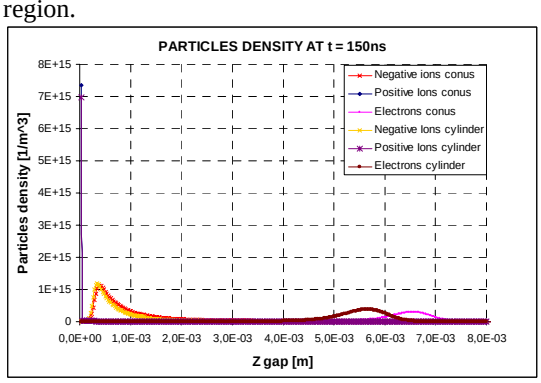

Fig. 6. Particles density at 150ns. Notice that negative ions and electron densities are located in different gap regions.

Meanwhile at 150ns (Fig. 6) particles densities start to become different. Positive ion density is located in the same interelectrodic gap space but it is higher for the conical discharge geometry ($7.34 \cdot 10^{15}$ [particles/m3]) than in the cylindrical discharge channel ($6.96 \cdot 10^{15}$ [particles/m3]). Negative ion density maximum is located in different interelectrodic gap regions: for the conical channel is $1.09 \cdot 10^{15}$ [particles/m3] at 0.4mm from the cathode, and for the cylindrical channel is $1.18 \cdot 10^{15}$ [particles/m3] at 0.3mm from the cathode. Electrons density for the conical channel is $2.98 \cdot 10^{14}$ [particles/m3] at 6.5mm from the cathode and in the cylindrical discharge channel is $3.8 \cdot 10^{14}$ [particles/m3] at 5mm from the cathode.

There are differences in the location of the particles densities due to the higher drift velocity of electrons and negative ions in the conical discharge channel. Electric field is higher in the conical discharge channel and negative ion and electron velocity are proportional to the

electric field magnitude.
In Trichel pulse decay phase (Fig. 7), the ionic charge density is higher in the conical discharge channel than in the cylindrical discharge channel; therefore, the external circuit current is higher in the conical geometry than in the cylindrical geometry as Fig. 2 shows. Electron density is higher for the cylindrical discharge channel than the conical discharge channel. Due to the higher velocity of electrons in the conical channel, electron density has reduced faster in the interelectrodic gap space because it is moving in a fewer electric field in the same time instant than in the cylindrical discharge channel.

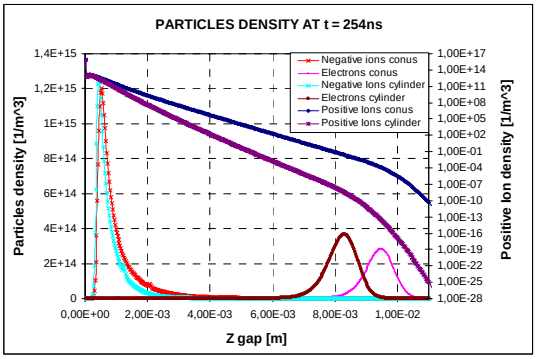

Fig. 7. Particles density at 254ns. Notice that ionic charge is the most important charge particle in the interelectrodic gap space, but conical particles magnitudes are higher than cylindrical particles magnitudes.

3. Discussion

With a conical discharge radius, particles density become higher and the electron drift velocity too; making that the external current acquires a higher peak value and direct current components.

The discussion is focused around the external circuit current behavior. The initial rapid rise in the current is due to electrons in the high electric field region near the electrode tip (cathode). A great number of electrons with high velocity are produced by ionization, giving a great rise in the current.

During the time when the current arises to its maximum value, electrons are the most important particle density in the interelectrodic gap distance. Then the current increase depends on the variation time of the electron density.

The current decays because a “dense plasma” region is formed. Between this plasma region and the cathode, positive ions dominated the space charge to form a cathode screening. Then, the decay of the current pulse can be considered as a formation process of an ionic charge density in the interelectrodic gap space.

The similar behavior of particles densities with the different discharge geometries demonstrates that electron growth (dominant part of the initial process) is developed in a small discharge radius, but this discharge radius does not grow with the interelectrodic gap distance because the measured current will be higher and it will have a different tail time.

4. Conclusion

In the coaxial arrangement, the geometrical discharge form is cylindrical; this means that the discharge is filamentary.
The discharge geometry determines the particles density and then the external circuit magnitude. Additionally, it changes the electric field behavior and this will determine important discharge characteristics as particles velocity, attachment, first ionization, and excitation coefficients, etc.

The cylindrical discharge channel simulation explains adequately the rise and fall current pulse and the direct current component based on the theory. It has been demonstrated that a plasma region is responsible of the current fall and the direct component.

Acknowledgments

Authors would like to thank Universidad Nacional de Colombia and COLCIENCIAS for the financial support of the present project *RC number 470 – 2003*

References

[1] Essam Nasser. Fundamentals of Plasma Gaseous ionization and plasma electronics. *Wiley – Interscience* 1971
[2] L. Loeb. Basic Process of Gaseous Electronics.

California university Press. 1961

[3] S. Badaloni and I. Gallimberti. Basic Data of Air Discharges. *Universita' di Padova 1972*

[4] R. Morrow. Theory of Negative Corona in Oxygen. *Phys. Rev.* A 32 Number 3 1799. September 1985

[5] Dancer, Davidson, Farish IEEE Meeting IAS, pp. 87 – 90.

[6] Reess and Paillol. The role of the field – effect emission in trichel pulse development in air at atmospheric pressure. *J. Phys, D. Appl. Phys. 30. 1997*

[7] A. Davies, C. Evans. . Field distortion in gaseous discharges between parallel – plate electrodes. *Proc. IEE*, Vol 124, N° 2, 1977

[8] N. Sato. Discharge Current Induced By The Motion Of Charged Particles. *J Phys. D: Appl. Phys*. 13, L3. 1980

[9] J. Boris and D. Book. Flux corrected transport. I. Shasta, a fluid transport algorithm that works. *J. Comp Phys.* 11, 38 – 69. 1973

[10] S. Zalesak. Fully Multidimensional Flux – Corrected Transport Algorithms For Fluids. *J of Comp Phys* 31, 363 – 378. 1979

[11] Arévalo, Díaz, López, Gómez, and Román. Corona Current Impedance…, 27th International Conference on Lightning Protection ICLP 2004.

[12] L. Arévalo, O. Díaz and F. Román Adding negative corona currents produced by independent electrodes. XIIIth International Symposium on High Voltage Engineering. 2003.